Surface & Coatings Technology 267 (2015) 90–97

Contents lists available at ScienceDirect

Surface & Coatings Technology

journal homepage: www.elsevier.com/locate/surfcoat

Silver surface segregation in Ag-DLC nanocomposite coatings

Noora Kristiina Manninen [a], Ramon Escobar Galindo [b], Sandra Carvalho [a,c], Albano Cavaleiro [a]

[a] SEG-CEMUC, Department of Mechanical Engineering, University of Coimbra, Coimbra 3030-788, Portugal
[b] Instituto de Ciencia de Materiales de Madrid (ICMM-CSIC), Cantoblanco, Madrid, Spain
[c] GRF-CFUM, Physics Department, University of Minho, Guimarães, Portugal

ARTICLE INFO

Available online 19 December 2014

Keywords:
magnetron sputtering
DLC
morphology
Ag surface segregation
Ag-alloyed DLC

ABSTRACT

AgDLC coatings were deposited by magnetron sputtering in order to evaluate: i) the Ag nanoparticle size distribution along the coatings thickness and ii) the silver stability in DLC coatings. Four different coatings were deposited, two AgDLC nanocomposite coatings containing 20 at.% of Ag, with thicknesses of 250 nm and 1000 nm, a 250 nm AgDLC nanocomposite coating with carbon barrier layer of 75 nm and a multilayer coating, consisting of a pure Ag layer with a carbon barrier layer of 75 nm. The coatings were characterized with respect to their structure (by means of X-ray diffraction (XRD)), morphology (by scanning electron microscopy (SEM)) and Ag distribution in depth (by glow discharge optical emission spectroscopy (GDOES)). The AgDLC nanocomposite coatings are composed of Ag nanograins (with a size of about 3 nm) dispersed in an amorphous carbon matrix. The SEM results suggest a bimodal size distribution along the coatings thickness, it was found that Ag forms nanoparticles and aggregates with sizes ranging from 14 nm up to 52 nm on the coating's surface, whereas in bulk, no Ag nanoparticles were visible by SEM. The monitoring of the Ag stability at room temperature conditions during a period of 6 months showed that Ag segregates to the coatings surface, in the AgDLC nanocomposite coating with 1000 nm forming Ag nanofibers, while the thinner AgDLC (250 nm) as well as the multilayer (Ag + DLC and AgDLC + DLC) coatings were stable over time.

1. Introduction

Diamond-like carbon (DLC) coatings are largely used as wear protective coatings, owing to their low friction coefficient and high hardness; moreover, these coatings are chemically inert, presenting outstanding corrosion resistance. Presently, carbon-based coatings find numerous industrial applications in different fields, namely, microelectronics, optics, manufacturing and biomedical devices [1]. The incorporation of different metal atoms (e.g. Ti [2], Zr [3], W [4], Cu [5], Ag [6–20], among others) enables us to tailor the carbon coating's functional properties, namely, the tribological behavior, residuals stress state and, consequently, the coating's adhesion, corrosion resistance, electrical resistivity and biological response [21]. In the particular case of silver-doped DLC, it has been reported that these coatings are able to i) reduce the residual stress state, thus improving the coating's adhesion to different substrates [9,13,18], ii) provide antibacterial properties [7,17] and iii) improve the tribological behavior [14,15,20]. AgDLC coatings have been pointed as an effective coating for biomedical implants due to their good corrosion resistance, wear resistance [7,20], antibacterial activity [7,17] and hemocompatibility [10]. Moreover, Endrino et al. [11] reported that amorphous carbon coatings containing about 5.5 at.% of Ag were not toxic against mouse MC3T3 osteoblastic cells.

Numerous studies report that AgDLC coatings are able to form nanocomposite coatings, where metallic Ag nanoparticles are dispersed in amorphous carbon matrix, with the size of these nanoparticles being strongly dependent on the deposition process and parameters and also on the amount of Ag incorporated in the carbon coating [7,9,14,15]. In fact, the functional properties of these nanocomposite coatings are determined by the size of Ag nanoparticles and their distribution along the coating's thickness; thus, in order to achieve the desired functional properties, the structure and morphology of these coatings must be precisely controlled. Previous works of the group suggested that Ag nanoparticles are not stable in DLC coatings, it was found that silver is able to diffuse and segregate in the coating's surface even at room temperature conditions, which had a strong influence on the tribological behavior [18]. The mobility of Ag in different nanocomposite coatings has been reported in numerous works, it was found that Ag forms a silver-rich layer on the coating's surface. Several reports state a nonuniform Ag distribution along the coating's thickness in as-deposited coatings, where a silver-rich layer is found on the coating's surface followed by an Ag depletion zone a few nanometers below the coating's surface [22–24]. The surface segregation of Ag has been used by several authors in high-temperature tribological applications, since it is claimed that Ag diffuses to the coating's surface during heat treatments at several hundred degrees, forming a lubricant surface layer [25–29]; however, in order to guarantee an extended service life, the Ag diffusion must be controlled. Muratore et al. [28] and Mulligan et al. [29] have proposed the use of diffusion barrier layers based on TiN and CrN coatings, with a designed morphology to allow an efficient Ag transport to the coating's surface. Moreover, the Ag surface segregation must exert a

http://dx.doi.org/10.1016/j.surfcoat.2014.12.029
0257-8972/

strong influence on the coating's antibacterial activity. Of particular importance is the metal ionization, since the bactericidal effect is associated with the release of Ag^+ ions, which requires direct contact between the biological medium and the Ag when present on the coating's surface.

In the present report, AgDLC coatings were deposited by dual dc magnetron sputtering and i) the Ag nanoparticles size distribution along the coating's thickness was determined and ii) the coating's morphology and stability over time in room temperature conditions were evaluated. Four different coatings were deposited i) and ii) AgDLC coatings with thicknesses of 250 nm and 1000 nm, respectively, and 20 at.% Ag; iii) AgDLC coating (thickness of 250 nm and 20 at.% Ag) with a DLC barrier layer of 75 nm on the top, in order to evaluate the effect of carbon layer on the growth of Ag clusters on the coating's surface; iv) for comparison with iii), a pure Ag layer was covered with a top DLC barrier layer. The main idea in the first two cases was to obtain coatings with different thicknesses and, consequently, with different morphologies, to analyze their influence on the Ag segregation rates. The coatings were characterized with respect to their morphology (SEM), structure (XRD) and chemical composition through coatings thickness (GDOES). The Ag surface segregation over time was evaluated by SEM and GDOES depth profiling analysis.

2. Experimental details

AgDLC coatings were deposited by dc magnetron sputtering onto polished and ultrasonically cleaned 316 L stainless steel (20×20 mm^2) and single crystalline silicon (100) substrates. The deposition chamber contains two opposite magnetrons and a rotatable substrate holder. The deposition system is pumped by rotary (Pfeiffer Vacuum, DUO 20 M) and diffusion (BOC Edwards-Diffstak 160/700) pumps to the base pressure of 5×10^{-4} Pa. Silver-doped DLC coatings were deposited using two targets (one pure C target (99.99%) and one pure Ag target (99.99%)), both with dimensions of 200 mm × 100 mm, in an Ar atmosphere. Before each deposition, the substrates were cleaned in ultrasonic baths in acetone, ethanol and distilled water, for 10 min in each solvent. In order to further improve the coating's adhesion to the substrate, an etching process was performed before each deposition in an argon atmosphere (Ar flow of 35 sccm) and by applying a pulsed dc bias voltage of 500 V to the substrate holder. Simultaneously, the C and Ag targets were connected to dc power supplies, and a power density of 1.75 W/cm^2 and 0.25 W/cm^2, respectively, were applied to the targets in order to eliminate contamination from their surface. During the etching process, the substrates were protected by a stainless steel shield. The depositions were performed with substrates rotating at 10 cm from the target with a constant speed of 18 rpm. A pulsed negative dc bias voltage of 50 V was applied to the substrate holder, and no additional heating was applied. During deposition, the Ar flow was kept at 42 sccm, which results in a deposition pressure of 5×10^{-1} Pa. The deposition of AgDLC coatings was performed by applying a power density of 7 W/cm^2 and 0.09 W/cm^2, to C and Ag targets, respectively. The deposition times were adjusted in order to vary the coating's thickness, as indicated in Table 1. For the deposition of AgDLC coating with DLC barrier layer, the deposition conditions were similar to the ones used for AgDLC coating; however, in order to deposit additional DLC layers, the Ag target was switched off during the last 9 min of deposition. The Ag + DLC bilayer coating was deposited by applying a power density of 0.25 W/cm^2 to the Ag target (for 35 min) and after the deposition of Ag layer a power density of 7 W/cm^2 was applied to the carbon target for 9 min. The deposition parameters are summarized in Table 1.

In order to determine the coating's chemical composition, electron probe microanalysis (EPMA), was performed in a Cameca SX 50 apparatus. Five punctual measurements were randomly performed on the samples' surface, with an acceleration voltage of 10 kV. The EPMA analysis was performed in AgDLC coating with a thickness of 1 μm, deposited on silicon substrate. The coating's morphology and thickness were evaluated by scanning electron microcopy (SEM) analysis in an EDAX-Nova nano-SEM200 equipment. The structural characterization was performed by x-ray diffraction (XRD) (in a PANalytical X'Pert PRO MPD diffractometer) operating with Cu Kα ($\lambda = 1.54060$ Å). The analysis was performed in grazing incidence mode with an angle of incidence of 1°. The Ag grain size was determined by Scherrer formula using the (111) peak [30]. The XRD peaks were fitted with pseudo-Voigt function, which allowed us to calculate either the full-width at half-maximum (FWHM) and the peak position (2θ). SEM (cross-sectional analysis) and XRD analysis were performed in AgDLC coatings deposited on silicon substrates.

In order to evaluate the coating's stability over time, the coatings surface was monitored by SEM analysis, every month, during a period of 5 months. The coatings were stored in atmospheric conditions, at about 25 °C. The top-view images were recorded in secondary electron (SE) and backscattered electron mode (BSE) mode. The SEM analysis was performed in different areas at different magnifications (starting from 25,000× up to 200,000×) in order to evaluate the coating's uniformity. The recorded SEM micrographs are representative of the coating's surface. The clusters mean size as well as the area coverage over time were evaluated by analyzing the SEM images (in SE mode with a magnification of 200,000×) in ImageJ software. Since the clusters' shape is not spherical, the major and minor dimensions were determined and only the particles with a major dimension above 10 nm were considered. The Ag aggregates and nanofibers were considered in the statistical analysis.

Glow discharge optical emission spectroscopy (GDOES) was performed in order to determine the depth profile of elements in as-deposited coatings and also 6 months after deposition. GDOES was performed in a Horiba Jobin Yvon RF GD Profiler equipped with a 4-mm diameter copper anode, operating at radiofrequency discharge pressure of 650 Pa (in argon atmosphere) and a power of 40 W. The coating's stability over time (determined by SEM top-view micrographs and GDOES analysis) were performed on the coatings deposited on SS316L substrates, which is a widely used material in different biomedical devices and mechanical components.

Table 1
Coatings deposition parameters, mean clusters size and Ag grain size.

Coating	Layer I					Layer II				Mean Size of Ag Clusters on Coating's Surface (nm)		Ag Grain Size (nm)
	J_{Ag} (W/cm^2)	J_C (W/cm^2)	Dep.Time (min)	Thickness (nm)	Ag Content (at.%)	J_C (W/cm^2)	Dep.Time (min.)	Thickness (nm)	Ag Content (at.%)	Minor	Major	
AgDLC-A	0.09	7	120	1000	20	–	–	–	–	52 ± 41	34 ± 23	~3
AgDLC-B	0.09	7	25	250	20	–	–	–	–	19 ± 6	14 ± 4	~3
AgDLC-B + DLC	0.09	7	25	250	20	7	9	75	0	–	–	~3
Ag + DLC	0.25	–	35	130	100	7	9	75	0	–	–	28

3. Results and discussion

3.1. Structural and morphological characterization of as-deposited AgDLC coatings

The coating's deposition parameters are summarized in Table 1, together with the chemical composition determined by EPMA, Ag clusters mean size determined from SEM top-view micrographs and Ag grain size, obtained from XRD analysis. The coatings were labeled as AgDLC-A and AgDLC-B, which represent the coatings with thicknesses of 1000 nm and 250 nm, respectively. The nanocomposite coating with an additional DLC barrier layer is labeled as AgDLC-B + DLC, since the deposition parameters used for the deposition of AgDLC nanocomposite layer were similar to those used for the deposition of coating AgDLC-B. As previously mentioned, the AgDLC nanocomposite coatings were deposited with similar deposition conditions, which leads to similar Ag contents in the coatings (20 at.% Ag); however, the deposition time was varied in order to obtain different thicknesses.

The SEM top-view and cross-sectional micrographs of the as-deposited coatings are depicted in Fig. 1.

The SEM top-view micrographs of coatings AgDLC-A (Fig. 1(a)) and AgDLC-B (Fig. 1(b)) suggest the presence of Ag nanoparticles embedded in the DLC matrix coating. The formation of Ag nanoclusters in amorphous carbon [7,9,14,15], TiCN [31], ZrCN [32] and TiO_2 [23] coatings were previously observed by several authors, and their formation was attributed to the lack of solubility of Ag in these ceramic matrixes [22]. Since the shape of these clusters is not spherical, their size is evaluated by determining the size along two axes, which are defined as minor and major. The mean cluster size determined by the analysis of top-view micrographs indicate that the Ag clusters mean size is 52 ± 41 nm (major), 34 ± 23 nm (minor) and 19 ± 6 nm (major), 14 ± 4 nm (minor), for AgDLC-A and AgDLC-B coatings, respectively. Regarding the cross-sectional SEM micrographs of AgDLC-A and AgDLC-B coatings depicted in Fig. 1(e) and (f), respectively, no evidence of Ag clusters is found, which suggests that the size of Ag clusters in the bulk is below the detection limit of SEM analysis. Since the top-view and cross-sectional micrographs of these coatings were performed with the same magnification (200,000×), it can be concluded that the particle size in the coating's surface and bulk are different. Chakravadhnula et al. [23] reported a bimodal Ag cluster size in Ag-TiO_2 coatings deposited by magnetron sputtering, where the size of Ag clusters embedded in the matrix were smaller (2 nm) than the size Ag clusters at the surface (7 nm). These authors proposed a two-step model to explain the bimodal distribution of Ag clusters along the coating's thickness, the first occurring during the deposition of Ag and TiO_2 and the second after the deposition process. During the co-deposition of Ag and C, the Ag atoms were deposited individually, being able to move in the surface forming islands/clusters, until the surface was covered by the growing carbon coating. In the coating's surface, Ag growth was not restricted by additional carbon layers and thus, bigger clusters were formed, a process which is thermodynamically favored by the reduction in the surface energy [23]. This theory is supported by the SEM top-view images, since no Ag clusters were found in the AgDLC-B coating covered by an additional DLC layer, contrarily to single AgDLC-B film. The top-view micrographs shown in Fig. 1 were recorded in BSE mode, which resulted in lower resolution in relation to SE mode analysis; however, since the thickness of the DLC top layer in coating AgDLC-B + DLC is 75 nm, which is higher than the depth analysis obtained in SE mode, the SEM micrographs were recorded in backscattered electron mode [33]. The evaluation of Ag nanoparticles size was performed using the SE micrographs (see Figs. 3 and 4; Section 3.2.1) due to the better resolution. It should be pointed out that the SEM micrographs were recorded two weeks after the coating deposition, thus, it is difficult to unequivocally determine if the Ag aggregates were formed during the deposition process or due to coatings ageing, specially taking into account the low stability of these coatings even at atmospheric conditions, as discussed below in Section 3.2 regarding Ag surface segregation.

Regarding the cross-sectional micrographs of coatings AgDLC-A and AgDLC-B, different morphologies can be observed, it is clear that the thinner coating presents a featureless morphology, revealing a compact and dense coating, while the thicker one shows a less compact morphology with a columnar growth. In fact, the changes in coatings morphology with the increase in deposition time and, consequently, in the thickness, have been previously reported [34–36]. Puchert et al. [34] reported that an increase in the coating's thickness enhances the probability of columnar growth and overshadowing, which also leads to the appearance of voids.

The coating's crystalline structure was evaluated by means of XRD and the results are shown in Fig. 2, where the main Ag diffraction peaks are identified (ICDD 181730).

According to the results depicted in Fig. 2, it can be found that the only crystalline phase detected in the coatings correspond to fcc-Ag in

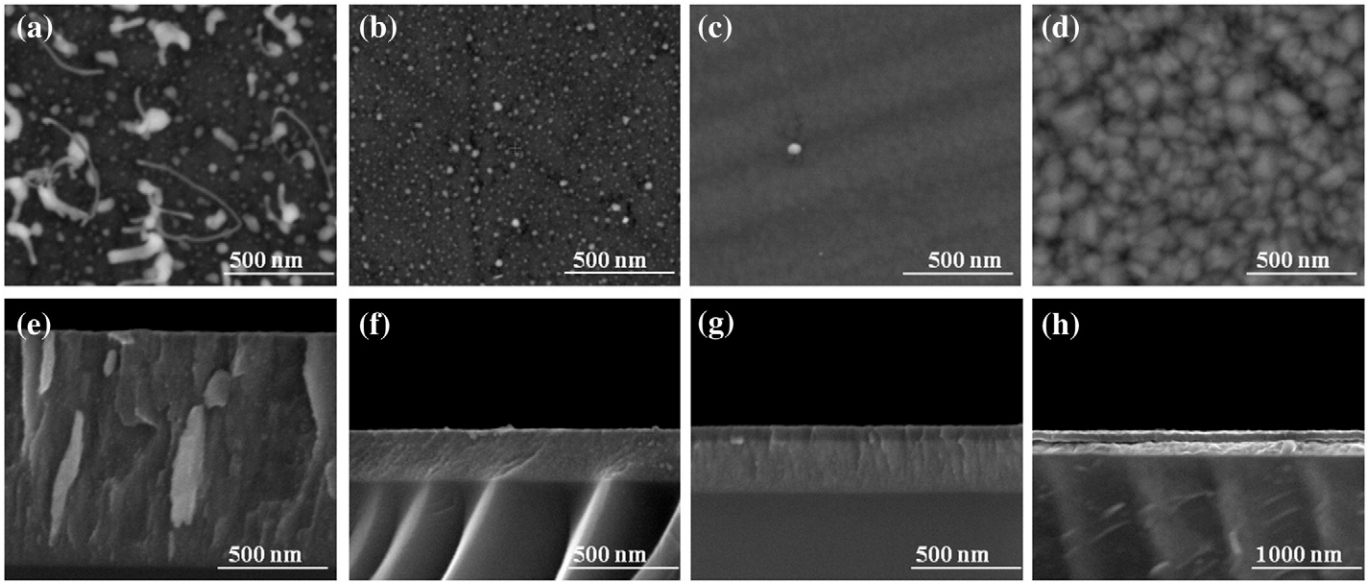

Fig. 1. SEM top-view micrographs (recorded in BSE mode) and cross-sectional micrographs (recorded in SE mode) of coatings (a), (e) AgDLC-A, (b), (f) AgDLC-B, (c), (g) AgDLC-B + DLC and (d), (h) Ag + DLC, respectively.

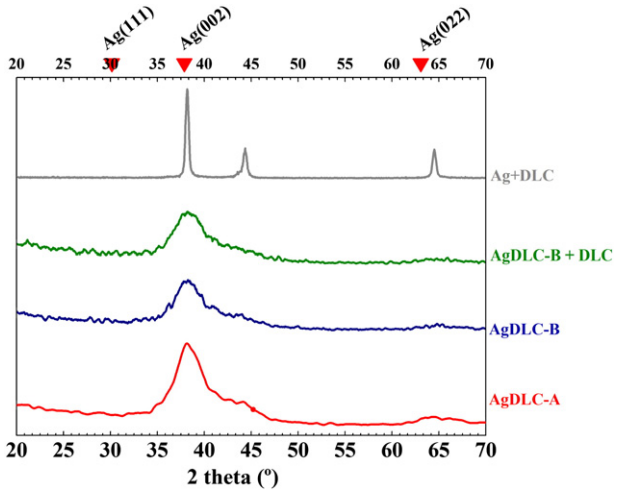

Fig. 2. XRD patterns of AgDLC coatings.

good agreement with our previous studies where the microstructure of these coatings was characterized by a random dispersion of Ag nanoparticles in an amorphous carbon matrix [18]. The grain size of Ag phase was determined by Scherrer formula, indicating the presence of small Ag grains with about 3 nm in both Ag-doped DLC coatings, while the Ag grain size in Ag + DLC coating was about 28 nm. The mean Ag particle size determined by the analysis of SEM micrographs suggested the presence of Ag particles with a mean size ranging from 19 nm to 52 nm and from 14 nm to 34 nm, for coatings AgDLC-A and AgDLC-B, respectively (see Table 1 and Fig. 1(a) and (b)), a value much higher than the grain size determined by the XRD analysis (about 3 nm). Thus, the results suggest that i) big Ag nanoparticles with dimensions of tens of nanometers are present in the coating's surface, which are composed of small grains of about 3 nm size or, ii) the Ag clusters distribution is not uniform through the coating's thickness, with small Ag clusters, with a mean diameter similar to the grain size (3 nm), formed in the bulk, while the clusters at the surface show a higher diameter. The last hypothesis is consistent with the differences found in top-view and cross-sectional micrographs, where no evidence of Ag clusters in the bulk was found. Taking into account that the depth of analysis in XRD is several hundred nanometers, even in a 1° glancing mode, the analysis regards mostly the coatings bulk because it is not possible to estimate the size of surface Ag grains.

3.2. Ag surface segregation

3.2.1. Evolution of Ag morphology over time

In order to evaluate silver stability in DLC, the coating's morphology was evaluated monthly by SEM analysis, during a period of 5 months. During this period, the coatings were stored at atmospheric conditions. The SEM top-view micrographs of coatings AgDLC-A and AgDLC-B are shown in Figs. 3 and 4, respectively. The area covered by Ag was evaluated over time, as well as the evolution in the Ag particle area (for coating AgDLC-B), and the results are shown on Fig. 5(a) and (b), respectively.

SEM micrograph of the coating AgDLC-A (Fig. 3(a)), indicates that the as-deposited coating surface is composed of i) spherical Ag clusters, ii) Ag aggregates and iii) Ag nanofibers, with a thickness of about 10 nm. From Fig. 3(b), (c) and (d) it can be concluded that the coating's surface changed with time, it was found that 3 months after deposition, the coating's surface is mainly composed of Ag fibers, although some Ag clusters and aggregates could still be found below these fibers. Moreover, it is clear that the amount of Ag on the coating's surface increases

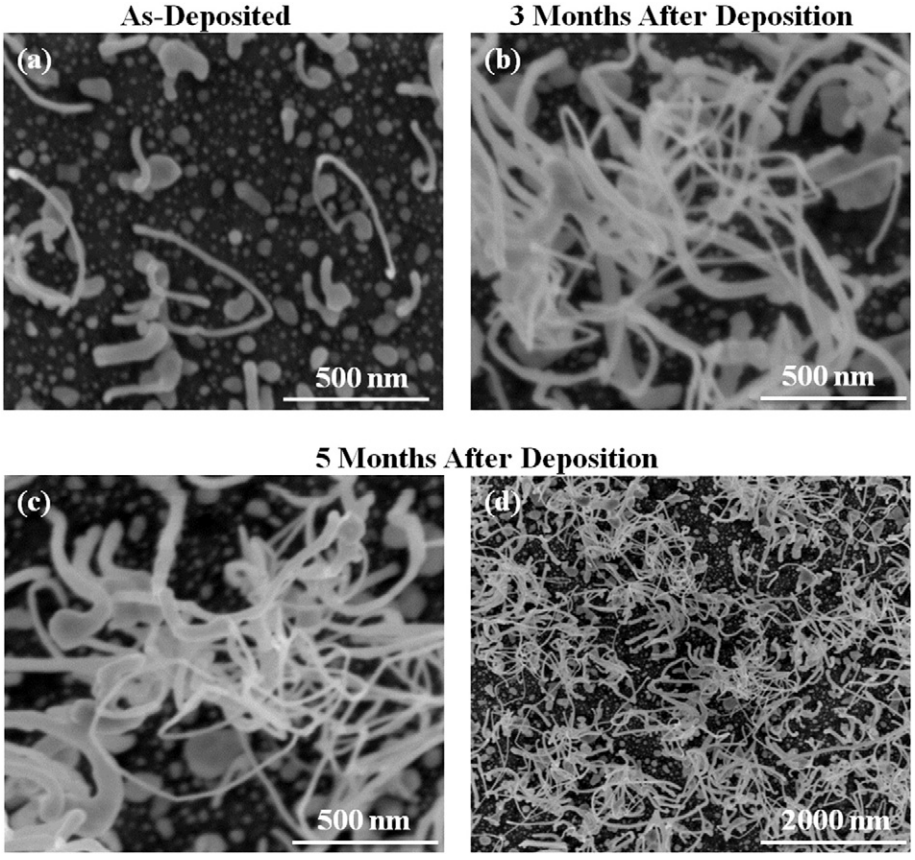

Fig. 3. SEM top-view micrographs (SE mode) of coating AgDLC-A (a) as-deposited, (b) 3 months after deposition, (c) 5 months after deposition and (d) lower magnification view of the coating's surface 5 months after deposition.

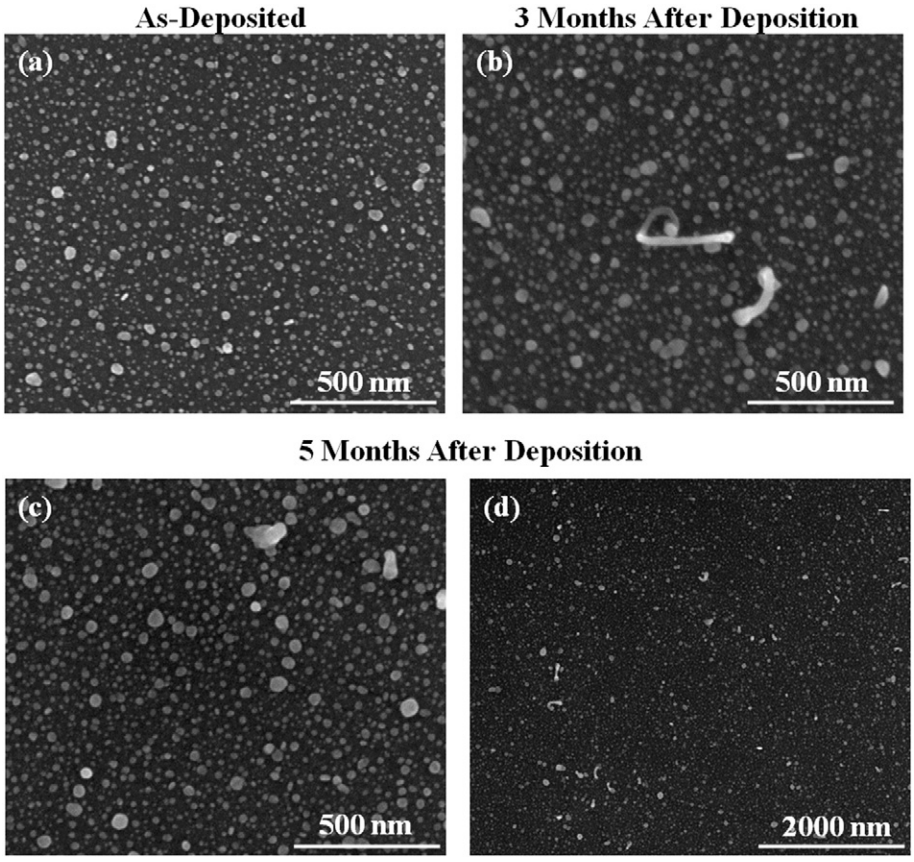

Fig. 4. SEM top-view micrographs (SE mode) of coating AgDLC-B (a) as-deposited, (b) 3 months after deposition, (c) 5 months after deposition and (d) lower magnification view of the coating's surface 5 months after deposition.

with time; the variations in surface area covered by Ag (Fig. 5(a)) indicate an increase from 26% to 60% for the first 3 months. Since the information obtained in SE mode is related to the first nanometers (5 nm to 50 nm) from the surface, the results suggest that silver segregates to the coating's surface, forming Ag nanofibers. It should be pointed out that similar observations in BSE mode (images are not shown) were found, which allows us to show elemental contrasts between carbon and silver, and confirms that these clusters and fibers are Ag.

Regarding the SEM micrograph of coating AgDLC-B (Fig. 4(a)), it can be found that the surface is mainly composed of spherical Ag nanoparticles, with a mean size of about 20 nm, combined with few Ag aggregates. The variations in surface area covered by Ag (see Fig. 5(a)) suggest that the amount of Ag is constant with time, thus indicating a different behavior in relation to coating AgDLC-A. The evolution of AgDLC-B coating is also different, suggesting the coalescence of Ag clusters which led to the formation of silver aggregates. Ag fibers emerging from the bulk are also visible but in a much lower extension when compared to the thicker coating. The mean size of Ag clusters is constant with time; however, the size distribution becomes wider over time, as can be found in the histogram on Fig. 5(b), which is attributed to the coalescence of surface Ag nanoparticles.

3.2.2. Ag depth profile and surface segregation

In order to evaluate the chemical composition of the coatings, depth profile GDOES analysis was performed in as-deposited and 6 months after deposition conditions. The Ag distribution is depicted in Fig. 6(a), (b), (c) and (d) for coatings AgDLC-A, AgDLC-B, AgDLC-B + DLC and Ag + DLC, respectively.

The GDOES depth profiles of as-deposited AgDLC coatings reveals that the Ag is uniformly distributed along the coating's thickness, with an average value close to 18 at.%. Regarding AgDLC-A coating, the Ag depth profile changed with time. Fig. 6(a) shows that an Ag-rich layer was formed on the coating's surface along with a decrease in the Ag content in the bulk (from 18 at.% to 14 at.%). Moreover, it can also be observed that the Ag content decreased through the entire coating thickness, which suggests that Ag is segregated from the entire coating thickness up to the coating's surface. Regarding coating AgDLC-B, the Ag depth profiles shown in Fig. 6(b) suggest that the coating is stable with time; neither the formation of an Ag-rich layer nor a reduction in the amount of Ag in the bulk were found. The results of GDOES analysis are consistent with the trends found with SEM analysis. Regarding AgDLC-B + DLC and Ag + DLC coatings, the GDOES depth profiles depicted in Fig. 6(c) and (d) indicate that no changes occurred in these coatings, which was also confirmed by SEM analysis (results not shown). In summary, three different behaviors were observed in different coatings: i) in AgDLC-A coating, the Ag segregates from the carbon matrix forming Ag nanofibers, which cover the coating surface a few months after deposition, ii) in AgDLC-B coating, the growth of surface Ag particles is observed with time and iii) the multilayer coatings with a DLC top layer are stable with time. It should be pointed out that the GDOES technique evaluates the thickness taking into account the theoretical density of the elements [37]. In case of sputtered coatings, it is well established that their densities do not correspond to the theoretical ones; in addition, DLC coatings present a very complex structure (which consists of a mixture of sp^1, sp^2 and sp^3 bonds), with the accurate density being very difficult to estimate [38]. Therefore, the thickness given in GDOES analysis can show discrepancies in relation to the real thickness. This is the reason why the thickness of both AgDLC-A and AgDLC-B coatings is different from the one measured by SEM (see Table 1 and Fig. 1). The errors associated with the evaluation of thickness by GDOES also explains why the integrated amount of Ag is different in AgDLC-A coating in the as-deposited and aged states. Still, the

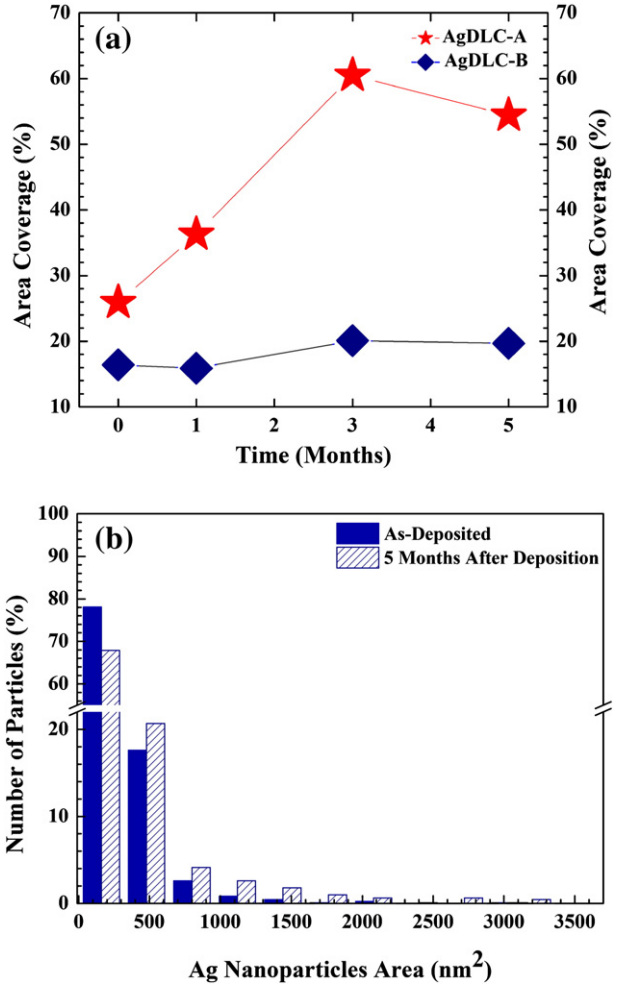

Fig. 5. (a) Variation of area covered by Ag with time in AgDLC-A and AgDLC-B coatings and (b) variation of Ag nanoparticle area with time in AgDLC-B coating.

GDOES depth profile allows us to prove the Ag segregation to the õsurface of the Ag-DLC films.

The influence of the particle diameter on the particle energy can be estimated by the Gibbs–Thompson relation, which allows us to determine the particle chemical potential (partial molar free energy) of an atom in a particle of radius r, ($\mu(r)$), which is given by:

$$\mu(r) - \mu(\infty) = \frac{2\Omega\gamma}{r}$$

Where $\mu(\infty)$ is the chemical potential in the bulk, γ is the surface free energy and Ω is the bulk metals volume per atom. This model predicts that the energy of a metal atom in a nanoparticle increases as the particles size decreases. Campbell et al. [39] experimentally determined the energy of Pb clusters and the authors found that the energy of a metal atom in a nanoparticle increases much more dramatically with decreasing size than predicted by Gibbs–Thompson relation. In fact, the high energy of these small nanoclusters explains their low stability, which leads to the cluster's growth in free surfaces, which seems to be the case in our coatings. This phenomenon has been reported by several authors, in metallic clusters deposited onto different substrates where the cluster's coalescence was found, and mainly controlled by the cluster's size and interaction between the clusters and the substrate [40–42]. Regarding the coating AgDLC-A, the results indicate that the Ag emerges from the bulk coating up to the surface, which means that Ag is diffusing inside the DLC matrix. The Ag surface segregation from CrN [26,27,29] and yttria-stabilized zirconia (YSZ) [25,28] coatings has been previously reported; however, this phenomena only took place at very high temperatures. Thus, the occurrence of Ag surface segregation in DLC coatings at room temperature was surprising and this suggests that the activation energy for Ag diffusion in carbon matrix is very low. In fact, the spontaneous growth of whiskers in electrodeposited Sn coatings, used for electronic components was reported over 50 years ago and this topic is still the subject of extensive study. The fundamental mechanisms controlling the formation of Sn whiskers is still not fully understood. Still, the most accepted hypothesis is that the whisker's growth is associated with stress relaxation [43]. In the case of AgDLC coatings, the driving force for this process is still not understood; however, it may be related to i) a decrease in the overall Ag cluster's surface area, associated with their growth; ii) reduction in the total system energy, due to the high energy associated with Ag-C interfaces or iii) reduction in Ag nanoclusters' stress state. The mechanism of Ag diffusion inside the carbon matrix still remains unclear; however, taking into account the different behaviors found in thin and thick coatings, some conclusions can be drawn. Both AgDLC-A and AgDLC-B coatings show a similar grain size inside the DLC matrix (with an average value of 3 nm) and the main difference between these coatings seems to be related with their morphology, which is columnar for the thick coating and featureless for the thin one (see Section 3.1). These differences suggest that the Ag diffusion is controlled by the DLC coating's morphology, Ag possibly diffusing through the column boundaries. Mulligan et al. [29] deposited CrNAg coatings with different CrN barrier layers and they found that the more compact CrN cap layers prevented the Ag surface segregation, inversely to what was observed for less compact ones. The faster Ag diffusion rates along the open columns interfaces in relation to the Ag diffusion through both the bulk CrN matrix and the CrN grain boundaries was the explanation for that behavior.

4. Conclusion

Silver-doped DLC coatings were deposited by dual dc magnetron sputtering and the Ag nanoparticles' size distribution along the coating's thickness and the coating's stability with time at atmospheric conditions were studied. Four different coatings were deposited i) and ii) AgDLC coatings with thicknesses of 250 nm and 1000 nm, respectively, and 20 at.% Ag; iii) AgDLC coating (thickness of 250 nm and 20 at.% Ag) with a DLC barrier layer of 75 nm on top, in order to evaluate the effect of carbon layer on the growth of Ag clusters on the coating's surface; iv) for comparison with iii), a pure Ag layer was covered with a top DLC barrier layer. AgDLC coatings have a nanocomposite structure, with Ag nanograins (with 3 nm measured by XRD), dispersed in an amorphous carbon matrix. The SEM top-view micrographs showed the presence of Ag clusters and Ag aggregates with sizes ranging from 14 nm up to 50 nm, while no evidence of Ag clusters was found by cross-sectional observation. These results allowed us to conclude that Ag nanoparticles have a bimodal size distribution through the coating's thickness. Moreover, since no Ag clusters are visible in the SEM top-view micrograph of the multilayer coatings with a DLC top barrier layer, it could be concluded that the Ag particle's mobility is restricted by the carbon layer, while in a free carbon surface, the silver particles are able to coalesce.

SEM results suggest a different behavior for the Ag stability in 1000 nm and 250 nm AgDLC nanocomposite coatings, it was found that Ag segregates to the surface in the thicker coating, forming Ag nanofibers, while the thinner one is stable with time. GDOES analysis showed a uniform Ag distribution through the coating's thickness in the as-deposited condition while the Ag depth profile of the aged AgDLC-A coating revealed the formation of an Ag-rich surface layer, along with a decrease in the Ag content from 18 at.% to 14 at.% in the entire coating thickness. All the other coatings were stable with time, behavior that was also confirmed by SEM analysis. The differences in the Ag stability in AgDLC nanocomposite coatings were attributed to their different thicknesses and morphologies; in fact, the thinner coating

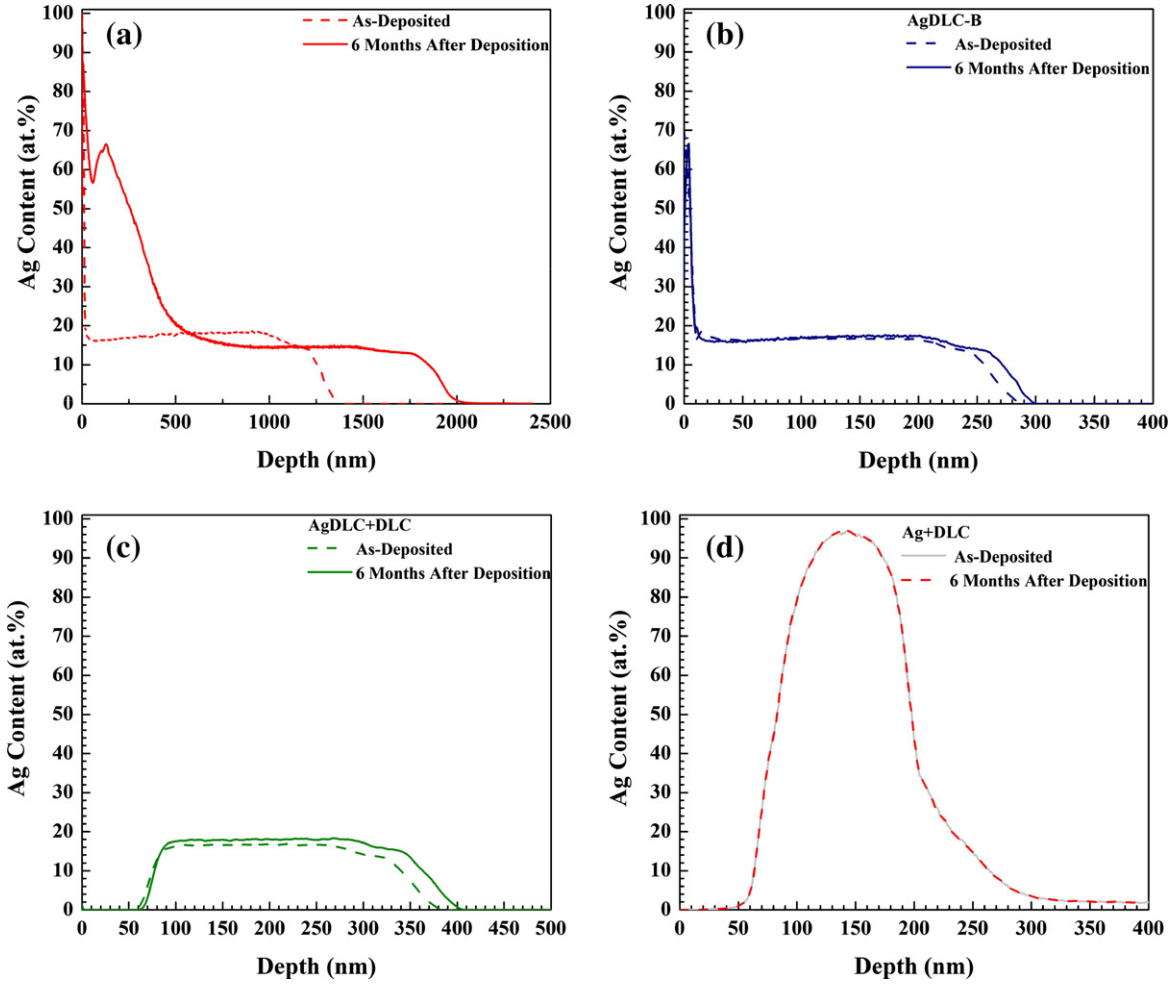

Fig. 6. GDOES depth profiles of Ag distribution in as-deposited coatings and 6 months after deposition for coatings (a) AgDLC-A, (b) AgDLC-B, (c) AgDLC-B + DLC and (d) Ag + DLC.

presented a more compact featureless morphology, while the thicker one was columnar.

Acknowledgments

FCT-Fundação para a Ciência e Tecnologia and FSE are acknowledged for the grant SFRH/BD/82472/2011. This research is sponsored by the FEDER funds through the program COMPETE-Programa Operacional Factores de Competitividade and by the national funds through FCT-Fundação para a Ciência e Tecnologia in the framework of the Strategic Projects PEST-C/EME/UIO0285/2011.

References

[1] C. Donnet, A. Erdemir, in: C. Donnet, A. Erdemir (Eds.), Tribology of Diamond-like Carbon Films, Springer, New York, 2008, pp. 1–10.
[2] A. Escudeiro, T. Polcar, A. Cavaleiro, Vacuum 85 (2011) 1144–1148.
[3] A. .Escudeiro, T. Polcar, A. Cavaleiro, Thin Solid Films 538 (2013) 89–96.
[4] C.W. Moura, J.R.T. Silva, A. Cavaleiro, Thin Solid Films 515 (2006) 1063–1068.
[5] R.M. Balestra, A.M.G. Castro, M. Evaristo, A. Escudeiro, P. Mutafov, T. Polcar, A. Cavaleiro, Surf. Coat. Technol. 205 (2011) 79–83.
[6] H. Biederman, P. Hlidek, J. PeSiEka, D. Slavinsk, V. Stundlia, Vacuum 47 (1996) 1385–1389.
[7] M.L. Morrison, R.A. Buchanan, P.K. Liaw, C.J. Berry, R.L. Brigmon, L. Riester, H. Abernathy, C. Jin, R.J. Narayan, Diamond Relat. Mater. 15 (2006) 138–146.
[8] G. Matenoglou, G.A. Evangelakis, C. Kosmidis, S. Foulias, D. Papadimitriou, P. Patsalas, Appl. Surf. Sci. 253 (2007) 8155–8159.
[9] H.W. Choi, J.H. Choi, K.R. Lee, J.P. Ahn, K.H. Oh, Thin Solid Films 516 (2007) 248–251.
[10] H.W. Choi, R.H. Dauskardt, S.C. Lee, K.R. Lee, K.H. Oh, Diamond Relat. Mater. 17 (2008) 252–257.
[11] J.L. Endrino, R. Escobar Galindo, H.S. Zhang, M. Allen, R. Gago, A. Espinosa, A. Anders, Surf. Coat. Technol. 202 (2008) 3675–3682.
[12] H.S. Zhang, J.L. Endrino, A. Anders, Appl. Surf. Sci. 255 (2008) 2551–2556.
[13] C. Wang, X. Yu, M. Hua, Appl. Surf. Sci. 256 (2009) 1431–1435.
[14] Y. Wang, J. Wang, G. Zhang, L. Wang, P. Yan, Surf. Coat. Technol. 206 (2012) 3299–3308.
[15] X. Yu, Y. Qin, C.B. Wang, Y.Q. Yang, X.C. Ma, Vacuum 89 (2013) 82–85.
[16] Y. Wu, J. Chen, H. Li, L. Ji, Y. Ye, H. Zhou, Appl. Surf. Sci. 284 (2013) 165–170.
[17] K. Baba, R. Hatada, S. Flege, W. Ensinger, Y. Shibata, J. Nakashima, T. Sawase, T. Morimura, Vacuum 89 (2013) 179–184.
[18] N.K. Manninen, F. Ribeiro, A. Escudeiro, T. Polcar, S. Carvalho, A. Cavaleiro, Surf. Coat. Technol. 232 (2013) 440–446.
[19] Š. Meškinis, et al., Surf. Coat. Technol. (2014). http://dx.doi.org/10.1016/j.surfcoat.2014.01.026.
[20] V. Dhandapani, E. Thangavel, M. Arumugam, K.S. Shin, V. Veeraraghavan, S.Y. Yau, C. Kim, D.E. Kim, Surf. Coat. Technol. 240 (2014) 128–136.
[21] J.C. Sánchez-López, A. Fernández, in: C. Donnet, A. Erdemir (Eds.), Tribology of Diamond-like Carbon Films, Springer, New York, 2008, pp. 311–338.
[22] R. Escobar Galindo, N.K. Manninen, C. Palacio, S. Carvalho, Anal. Bioanal. Chem. 405 (2013) 6259–6269.
[23] V.S.K. Chakravadhanul, C. Kubel, T. Hrkac, V. Zaporojtchenko, T. Strunskus, F. Faupel, L. Kienle, Nanotechnology 23 (2012) 495701 (7 pp.).
[24] J.E. Krzanowski, J.L. Endrino, J.J. Nainaparampil, J.S. Zabinski, J. Mater. Eng. Perform. 13 (4) (2004) 439.
[25] J.J. Hu, C. Muratore, A.A. Voevodin, Compos. Sci. Technol. 67 (2007) 336–347.
[26] C.P. Mulligan, D. Gall, Surf. Coat. Technol. 200 (2005) 1495–1500.
[27] L. Incerti, A. Rota, S. Valeri, A. Miguel, J.A. García, R.J. Rodríguez, J. Osés, Vacuum 85 (2011) 1108–1113.
[28] C. Muratore, J.J. Hu, A.A. Voevodin, Thin Solid Films 515 (2007) 3638–3643.
[29] C.P. Mulligan, T.A. Blanchet, D. Gall, Surf. Coat. Technol. 205 (2010) 1350–1355.
[30] P. Scherrer, N.G.W. Gottingen, Math.Phys. Kl. 2 (1918) 96.
[31] N.K. Manninen, R. Escobar Galindo, N. Benito, N.M. Figueiredo, A. Cavaleiro, S. Carvalho, J. Phys. D Appl. Phys. 44 (2011) 375501.
[32] S. Calderon, R. Escobar Galindo, N. Benito, C. Palacio, A. Cavaleiro, S. Carvalho, J. Phys. D Appl. Phys. 46 (2013) 325303 (10 pp.).
[33] S. Amelinckx, D. Dyck, G. Tendeloo (Eds.), Handbook of Microscopy Applications in Materials Science Solid-State Physics and Chemistry, VCH, Germany, 1997, p. 550.
[34] M.K. Puchert, P.Y. Timbrell, R.N. Lamb, J. Vac. Sci. Technol. A 12 (3) (1994) 727.
[35] R. Messier, R.C. Ross, J. Appl. Phys. 53 (9) (1982) 7656.

[36] C.E. Sittner, A. Bergauer, H. Bangert, W. Bauer, J. Appl. Phys. 82 (1995) 449.
[37] R. Payling, D. Jones, A. Bengston (Eds.), Glow Discharge Optical Emission Spectrometry, Wiley, 1997.
[38] J. Robertson, Mater. Sci. Eng. R37 (2002) 129–281.
[39] C.T. Campbell, S.C. Parker, D.E. Starr, Science 298 (2002) 811–814.
[40] S.J. Carrol, K. Seeger, R.E. Palmer, Appl. Phys. Lett. 72 (1998) 305.
[41] P. Deltour, J.L. Barrat, P. Jensen, Phys. Rev. Lett. 78 (24) (1997) 4597.
[42] N.K. Manninen, N.M. Figueiredo, S. Carvalho, A. Cavaleiro, Plasma Process. Polym. 11 (2014) 629–638.
[43] E. Chason, N. Jadhav, F. Pei, E. Buchovecky, A. Bower, Prog. Surf. Sci. 88 (2013) 103–131.